Energy Engineering

Tech Science Press

Doi:10.32604/ee.2025.074667

ARTICLE

Two-Stage Robust Optimal Dispatch of Integrated Wind-Solar-Hydro-Thermal-Storage System Containing P2G-CCS Equipment under Renewable Energy Uncertainties

Jiyuan Liao[1], Jiangyan Zhao[2,*], Xin Li[3], Changmao Liu[1], Banghong Tang[1] and Zihan Ling[3]

[1]Guizhou Wujiang Hydropower Development Co., Ltd., Guiyang, 550002, China
[2]Power China Guiyang Engineering Corporation Limited, Guiyang, 550081, China
[3]School of Electrical Engineering and Renewable Energy, China Three Gorges University, Yichang, 443002, China

*Corresponding Author: Jiangyan Zhao. Email: zhaojy01_gyy@powerchina.cn

Received: 15 October 2025; Accepted: 17 December 2025; Published: 06 August 2026

ABSTRACT: To address the uncertainty and volatility of renewable energy while meeting the requirements of low-carbon economic operation, this paper proposes a two-stage robust optimal dispatch model for an integrated wind-solar-hydro-thermal-storage energy system with coupled power-to-gas (P2G) and carbon capture system (CCS). First, a mathematical model of the integrated wind-solar-hydro-thermal-storage energy system with P2G-CCS coupling is developed to promote internal carbon cycling and enhance the capability to accommodate renewable energy. Second, the scheduling problem is formulated as a two-stage robust optimization model. A cardinality-based uncertainty set is adopted to model deviations in renewable energy output, and a column-and-constraint generation (C&CG) algorithm is applied to efficiently solve the problem. Comparative case studies are conducted to quantify the performance differences between the proposed method and deterministic optimization and stochastic optimization. The results show that compared with conventional optimization methods, the proposed two-stage robust optimization model increases the carbon utilization rate of the IES to 24.38% and raises the renewable energy accommodation rate to 100%; the system's intraday balancing cost and total operating cost are reduced by 94.54% and 4.49%, respectively, and the overall indirect carbon emissions decrease by 57.96%, thus achieving coordinated optimization of economic performance, robustness, and low-carbon characteristics. In addition, further analysis of the robustness parameter indicates that an overly conservative robust strategy leads to worse economic performance and higher carbon emissions. This study provides quantitative guidance for balancing robustness, economy, and environmental benefits in integrated energy system operation.

KEYWORDS: Integrated wind-solar-hydro-thermal-storage system; two-stage robust optimization; uncertainty; P2G-CCS; renewable energy; low-carbon economic dispatch

1 Introduction

As global warming and energy crises garner increasing attention, renewable energy development has become a crucial pathway for securing clean energy supply and advancing the low-carbon transformation of power systems [1]. However, renewable energy sources such as wind and solar power are inherently intermittent and fluctuating, making it challenging for single-energy systems to accommodate high proportions of renewables while ensuring reliable and economical power supply. As a multi-energy co-generation system, the integrated "wind-solar-hydro-thermal-storage" system can enhance renewable energy consumption while improving power system operational reliability and the low-carbon economic efficiency of energy utilization [2,3]. While existing research has made progress in optimizing the dispatch of integrated systems, it remains inadequate in addressing the uncertainty of renewable energy output. Furthermore, under high renewable penetration, the regulation capability of multi-energy coupled units such as electric-thermal units is constrained, limiting their full potential for integration and synergistic advantages. Therefore, enhancing system flexibility to further increase renewable energy integration levels and reduce carbon emissions represents an urgent and critical challenge [4–7].

Combined heat and power (CHP) serves as a mature and efficient electricity-heat coupling technology within IES, capable of simultaneously generating electricity and thermal energy based on load demands [8]. However, the uncertainty of renewable energy output and the operational constraints of conventional heat-driven CHP units limit the integration level of renewable energy [9]. To alleviate this contradiction, several emerging energy technologies have attracted extensive attention from academia and industry. These innovations break the physical isolation between traditional energy systems, aligning more closely with renewable energy development trends [10,11]. Among these, P2G technology utilizes surplus electricity to produce hydrogen or synthetic natural gas (SNG), enabling the conversion of electrical energy into gaseous energy while deepening the coupling between power grids and natural gas networks. This represents a potentially effective pathway to enhance renewable energy integration within integrated energy systems [12,13]. Wang et al. developed an economic, low-carbon, and clean dispatch model incorporating thermal power, natural gas, wind power, and P2G facilities [14]. In P2G reactions, carbon dioxide serves as the primary carbon source for methane production and plays a crucial role. However, most existing P2G studies have paid little attention to the origin of CO_2. Addressing this issue, Zhang and Zhang. developed a synergistic optimization model for P2G-CCS power plants, demonstrating that CO_2 captured by carbon CCS can serve as a high-quality carbon source for the P2G process [15]. Consequently, Ma et al. proposed a modeling and optimization scheduling method integrating P2G and CCS into CHP systems. Results indicated that after configuring these systems, wind and solar power integration capacities increased by 25.46% and 30.28%, respectively. while CO_2 emissions decreased by 177.65 t due to the capture and utilization of CO_2 from the CHP units for the P2G process. However, this study employed a deterministic scheduling framework and did not investigate the combined impact of wind and solar output uncertainty on system economics, robustness, and environmental benefits [16]. The aforementioned study demonstrated the feasibility of integrating P2G-CCS systems into integrated energy systems through aspects such as scheduling model construction, carbon source supply pathways, and system structural evolution. However, constrained by the inherent intermittency and volatility of renewable energy alongside the "heat-driven electricity generation" operation mode of traditional CHP units, integrated energy systems face dual challenges in practical operation: while simultaneously constrained by the rigid coupling characteristics of conventional CHP units, making stable operation challenging. Furthermore, existing studies predominantly operate within deterministic frameworks, neglecting the uncertainty of renewable energy output and the resulting risks of source-load imbalance. Consequently, comprehensive assessments of the economic viability and safety of integrated energy systems under uncertain conditions remain incomplete.

Research on uncertainty optimization primarily revolves around two typical approaches: stochastic optimization and robust optimization [17]. Stochastic optimization requires sampling scenarios based on the probability distribution of uncertain variables, transforming the uncertain problem into a deterministic one through scenario methods, and then solving the deterministic problem [18]. However, obtaining precise probability distributions for uncertain variables is often challenging, and computational time for stochastic optimization increases rapidly with the number of scenarios [19]. Unlike stochastic optimization, static robust optimization requires only describing the range of variation for uncertain variables through uncertainty sets, resulting in a relatively simpler modeling process with good stability [20]. Despite its advantages in handling uncertainty, static robust optimization necessitates pre-determining a feasible decision set across the entire uncertainty set during the planning phase. This approach uses worst-case scenarios as constraint boundaries to ensure system safety, typically requiring safety margins in power generation or electricity procurement decisions. Consequently, it often leads to reduced economic efficiency and conservative operational strategies [21]. Compared to static robust optimization models, adaptive robust optimization distinguishes between prior decisions and compensatory decisions. This allows compensatory decisions to adjust based on the actual outcomes of uncertainty, thereby preserving necessary operational flexibility while accounting for uncertainty [22]. Thus, adaptive robust optimization offers advantages over static robust optimization by reducing redundant reserves and conservative margins while ensuring worst-case feasibility, making it more suitable for power system optimization dispatch problems [23–25]. Furthermore, two-stage robust optimization can be viewed as an implementation form of adaptive robust optimization. By dividing decisions into a first-stage a priori decision and a second-stage compensatory decision solved after uncertainty is revealed, it characterizes the response process of the dispatch scheme to the realized outcomes of uncertainties. This ensures feasibility under the worst-case scenario within the uncertainty set while preserving necessary adjustment space. Compared to static robust optimization, this approach reduces decision conservatism and is suitable for modeling operational scheduling in systems incorporating large-scale renewable energy [26,27].

Thus, two-stage robust optimization has emerged as a key method for addressing uncertain scheduling in energy systems, finding application across diverse operational scenarios [28]. Liu et al. proposed a two-stage robust optimal dispatch model for microgrids considering a time-of-use pricing mechanism [29]. Li et al. proposed a multi-timescale coordinated control strategy based on two-stage robust optimization to address source-load mismatch and multi-timescale fluctuations in high-penetration PV bases. This approach reduces operational costs and curtailment rates through synergistic regulation of hydrogen storage, electrochemical storage, and demand response. However, the model does not account for multi-energy coupling factors, and its engineering applicability requires further validation [30]. Li et al. addressed the economic operation of Combined Cooling, Heating, and Power microgrids with P2G units under uncertain wind power output by constructing a two-stage robust optimization dispatch model based on data-driven uncertainty sets. Demand response was incorporated to coordinate multi-energy flows, reduce operating costs, and enhance wind power integration. However, the model treated wind power forecasting errors as the primary uncertainty source and provided a simplified characterization of P2G [31]. Wang et al. proposed a robust dispatch optimization method for wind–thermal–storage systems based on a hybrid carbon trading mechanism, so as to improve the rationality of carbon emission allowance allocation and reduce the instability of power systems with large-scale wind power integration [32]. Most of the above studies focus on balancing robustness and economic efficiency, lacking systematic analysis of the environmental impact of scheduling schemes, making it difficult to meet the operational requirements of low-carbon development. However, under low-carbon economic operation, robustness, economic efficiency, and environmental benefits should be regarded as key indicators for designing and evaluating integrated energy system dispatch plans. Therefore, for the IES incorporating P2G and CCS constructed in this paper, there is an urgent need to establish a global optimization framework that comprehensively considers safety and stability, economic efficiency, and green low-carbon performance.

In response to the aforementioned shortcomings, this paper proposes a two-stage robust optimization dispatch strategy that considers the uncertainty of renewable energy. By deploying electric boilers, gas boilers, and thermal energy storage to share heating demands, the rigid constraint of "heat-driven power generation" in CHP units is mitigated, achieving thermal-electric decoupling. Budget uncertainty sets are employed to characterize forecasting errors in wind and solar power generation, thereby deriving optimal operational decisions for the integrated "wind-solar-hydro-thermal-storage" system under worst-case scenarios. Finally, through two-stage robust optimization, the synergistic relationship among economic efficiency, robustness, and environmental benefits in the integrated "wind-solar-hydro-thermal-storage" system is investigated. Thus, the main contributions of this paper are as follows:

(1) Constructing an IES model incorporating P2G-CCS and CHP units, integrating the electricity-gas-heat multi-energy network, energy conversion units, and energy storage units within a unified framework. This model characterizes the role of P2G-CCS in carbon capture and SNG production, as well as the synergistic operational characteristics of CHP units in thermal-electric decoupling and carbon recycling, providing foundational support for subsequent robust optimization scheduling modeling.
(2) Addressing the uncertainty in wind and solar power generation, we utilize budget uncertainty sets to describe the randomness and volatility of wind and solar outputs. A two-stage robust optimization dispatch model suitable for the wind-solar-hydro-thermal-storage integrated system is developed, incorporating electricity, gas, and heat multi-energy flows, as well as electricity-heat storage behaviors into a unified constraint system. This model enables the coordinated optimization operation of the multi-energy coupled system under different risk preferences.
(3) The two-stage robust optimization dispatch problem with P2G-CCS is equivalently reformulated as a mixed-integer linear master-subproblem structure. The Column and Constraint Generation (C&CG) algorithm is introduced for solution, reducing model size and enhancing computational efficiency while ensuring worst-case feasibility. Case study results demonstrate that this robust scheduling model exhibits superior economic performance and robustness compared to stochastic and deterministic optimization approaches.
(4) Building on the integration of P2G-CCS, this study quantitatively analyzes the interplay between economic efficiency, robustness, and environmental benefits in integrated energy systems by adjusting robust tuning parameters. It examines the impact of carbon footprint variations and renewable energy penetration rates on system economics, providing dispatch decision support for low-carbon economic operation of integrated "wind-solar-hydro-thermal-storage" systems incorporating P2G-CCS under uncertain conditions.

The remainder of this paper is constructed as follows. Section 2 presents the general layout and energy flow framework of the constructed integrated energy system. Section 3 provides a detailed modeling of the system and converts the two-stage robust optimal dispatching problem to solve it. Section 4 conducts case study. Section 5 summarizes the conclusions.

2 Component Description

2.1 Structure of Integrated Wind-Solar-Hydro-Thermal-Storage System with P2G-CCS

As shown in Fig. 1, the integrated energy system constructed in this paper consists of the power network, natural gas network, and heating network, Within the power network, the IES utilizes hydropower stations and wind and photovoltaic power generation units in renewable energy sources as the main power sources. CHP serves as a crucial supplementary power source, generating electricity while providing heating to enhance primary energy utilization efficiency. When renewable energy output is insufficient, electric energy storage (EES) compensates for the power deficit by discharging. During periods of excess electricity, part of the power drives P2G-CCS. Additionally, this excess electricity can be converted into thermal energy via electric boiler (EB) or stored in EES to balance power demand across different time periods, thereby strengthening the power network's adaptability to renewable energy fluctuations.

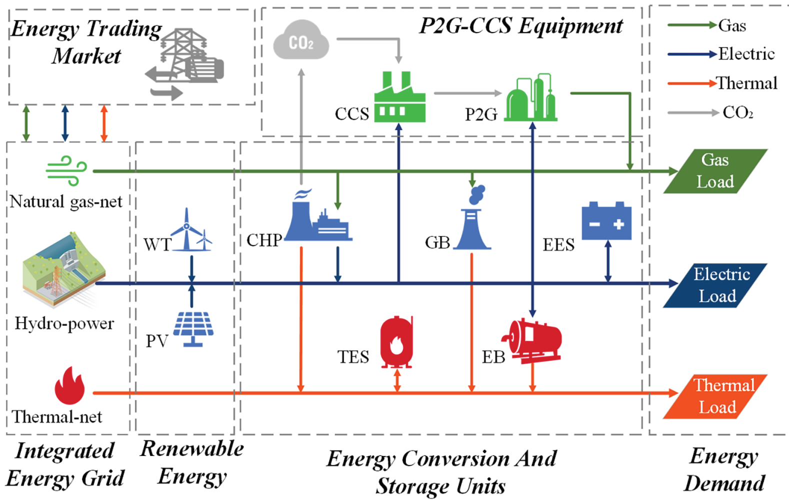

Figure 1: The configuration of the IES

Within the natural gas network, the IES procures natural gas from energy trading markets as the primary gas source, providing stable fuel for both CHP and gas boiler (GB). The P2G-CCS unit synthesizes high-quality methane using surplus electricity and carbon dioxide captured during the carbon capture process. This synthetic natural gas is reinjected into the natural gas network, jointly meeting gas load supply with externally purchased natural gas. This creates a diversified gas supply structure while achieving electrical coupling and carbon recycling at the gas network level.

Within the thermal network, CHP units serve as the primary heat source, delivering stable thermal energy to heat loads via the thermal pipeline network. Electric boilers and gas boilers, respectively convert electricity to heat and gas to heat. These are complemented by thermal energy storage (TES) systems that store and release surplus or off-peak heat at different times, smoothing thermal load fluctuations and reducing the rigid constraints imposed by "heat-driven electricity generation" operations. Through diversified heat source configuration and time-scale storage-release regulation, the thermal network ensures heating security while providing additional regulatory capacity for the electricity and natural gas networks.

Comprehensively, this IES relies on the coordinated operation of electricity, gas, and heat networks alongside energy conversion and storage components. Establishing a "capture-conversion-utilization" carbon cycle mechanism through P2G-CCS. This enables coordinated supply of electricity, gas, and heat loads under fluctuating renewable energy generation, enhancing system regulation capacity and energy supply reliability while reducing carbon intensity and overall operational costs. It provides structural and mechanistic support for achieving low-carbon economic operation in integrated energy systems.

2.2 The Main Operation Process of P2G-CCS

In addition, this paper constructs the P2G-CCS joint operation equipment with reference to the model proposed in the literature [33], which will convert excess renewable energy to natural gas. The P2G-CCS equipment primarily consists of a CCS section and a P2G section. The CCS section includes an absorber, a separator, and a carbon storage tank, responsible for separating and capturing CO_2 from the flue gas emitted by the integrated energy system. The P2G section comprises an electrolyzer and a Sabatier reactor, tasked with converting electrical energy into hydrogen and synthesizing natural gas with the captured CO_2. The operational flow is illustrated in Fig. 2. CO_2-containing flue gas first enters the absorber tower, where it comes into full contact with an amine solution containing monoethanolamide. CO_2 is absorbed to form a rich solution. After leaving the absorber tower, the rich solution undergoes exchange with the lean solution before entering the separator and distillation tower. During the heated stripping process, high-purity CO_2 is separated from the rich solution. The stripped solution returns to the absorber tower as lean solution for reuse. The separated CO_2 is compressed, with a portion transported to carbon storage tanks or secure locations for sequestration, while the remainder is fed into the P2G unit for natural gas synthesis. The P2G unit utilizes surplus electricity from wind and solar power to drive electrolysers that split water into hydrogen and oxygen. The hydrogen is then fed into a Sabatier reactor, where it reacts with CO_2 captured by the CCS system to produce synthetic natural gas. This synthetic gas supplements conventional natural gas supplies or meets gas load demands.

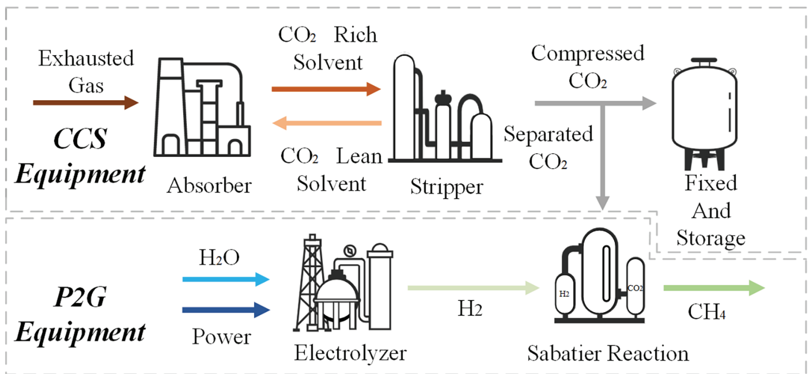

Figure 2: The main operation process of P2G-CCS equipment

Through this coupling approach, the P2G unit directly utilizes CO_2 captured by CCS as a carbon source, eliminating CO_2 leakage risks associated with long-distance transportation. It also avoids the need to purchase additional CO_2 from carbon markets, thereby reducing material costs for the P2G methanation reaction to some extent and mitigating economic and environmental challenges faced by traditional CCS and P2G schemes.

3 Model Formulation

In this section, to accurately describe the operational characteristics of each unit within the IES while ensuring efficient solution of the scheduling model, mature and conventional mathematical unit models are selected to represent the P2G-CCS system and related energy conversion and storage units. These models accurately capture the overall system behavior at low computational cost and align with engineering requirements in practical applications. By adopting these models, this paper effectively addresses key challenges in integrated energy system scheduling. It fully leverages the regulation capabilities and energy conversion properties of each unit while effectively managing the impacts of renewable energy output uncertainty and internal multi-energy coupling characteristics on system scheduling.

3.1 P2G-CCS Model

The rate of H_2 produced by the electrolyzer is shown in Eq. (1). $Q_{H_2,t}^{EL}$ is the amount of H_2 produced in the t period; $P_{ele,t}^{EL}$ is the power of the electrolyzer. η_{EL} represents the efficiency of the electrolyzer, and H_g is the calorific value of H_2. Eq. (2) describes the upper and lower power limits of the P2G.

$$Q_{H_2,t}^{EL} = \frac{\eta_{EL} P_{ele,t}^{EL}}{H_g} \tag{1}$$

$$P_{ele,min}^{EL} \le P_{ele,t}^{EL} \le P_{ele,max}^{EL} \tag{2}$$

Eq. (3) represents the relationship between the pure CO_2 captured by CCS and the exhausted gas emitted from the CHP unit. η_{CCS} is the carbon capture efficiency of CCS. ρ_{CO_2} is the CO_2 gas density. $Q_{CO_2,t}^{CCS}$ is the pure CO_2 captured by CCS, and $Q_{CO_2,t}^{CHP}$ is the exhausted gas emitted from the CHP unit in the t period.

Eq. (4) expresses the relationship between the CO_2 uncaptured by CCS and the exhausted gas emitted from the CHP unit.

$$Q_{CO_2,t}^{CCS} = \eta_{CCS} Q_{CO_2}^{CHP} \cdot \frac{1000}{\rho_{CO_2}} \tag{3}$$

$$Q_{CO_2,t}^{XCCS} = (1 - \eta_{CCS})\, Q_{CO_2,t}^{CHP} \tag{4}$$

The total power of CCS is the sum of the power consumed by CCS to capture CO_2 and the power consumed by CCS to fix CO_2. As shown in Eq. (5), $P_{ele,t}^{CCS}$ is the electric power consumed by CCS; $P_{fix,t}^{CCS}$ is the power consumed by CCS to fix CO_2; $P_{cap,t}^{CCS}$ is the electric power consumed by CCS to capture CO_2.

$$P_{ele,t}^{CCS} = P_{fix,t}^{CCS} + P_{cap,t}^{CCS} \tag{5}$$

Eq. (6) describes the relationship between the pure CO_2 captured by the CCS and the electrical power consumed for the capture in the t period. λ_{CCS} is the capture efficiency of the CCS.

$$P_{cap,t}^{CCS} = \lambda_{CCS} Q_{CO_2,t}^{CCS} \tag{6}$$

The pure CO_2 captured by the CCS is first synthesize into CH_4 by methanation in the P2G equipment, and the remainder is transferred and stored in a safe place as shown in Eq. (7).

$$Q_{CO_2,t}^{CCS} = Q_{CO_2,t}^{ME} + Q_{CO_2,t}^{STO} \tag{7}$$

Eqs. (8) and (9) describe the molar relationship between CH_4 synthesized in the sabatier reactor corresponding to H_2 and CO_2, respectively.

$$Q_{CH_4,t}^{ME} = \mu Q_{H_2,t}^{EL} \tag{8}$$

$$Q_{CH_4,t}^{ME} = \lambda Q_{CO_2,t}^{ME} \frac{\rho}{1000} \tag{9}$$

3.2 Energy Conversion & Storage Model

(1) CHP operating constraints

$$\begin{cases} P_{ther,min}^{CHP} \le P_{ther,t}^{CHP} \le P_{ther,max}^{CHP} \\ P_{ele,t}^{CHP} \ge P_{ele,min}^{CHP} - k_1^{CHP} P_{ther,t}^{CHP} \\ P_{ele,t}^{CHP} \le P_{ele,max}^{CHP} - k_2^{CHP} P_{ther,t}^{CHP} \\ P_{ele,t}^{CHP} \ge k_3^{CHP} P_{ther,t}^{CHP} \end{cases} \tag{10}$$

Eq. (10) describes the upper and lower limits of the heat output of the CHP and the "heat-and-power" operation constraints. $P_{ther,t}^{CHP}$ is the thermal power output of CHP unit. $P_{ele,t}^{CHP}$ is the electric power output of CHP unit. $P_{ele,min}^{CHP}$ is the minimum electric power. $P_{ele,max}^{CHP}$ is the maximum electric power. k_1^{CHP}, k_2^{CHP} and k_3^{CHP} are the conversion efficiency between thermal and electric energy.

(2) Gas boiler operational constraints

$$P_{ther,min}^{GB} \le P_{ther,t}^{GB} \le P_{ther,max}^{GB} \tag{11}$$

$$P_{ther,t}^{GB} = \lambda_{NG} Q_{gas,t}^{GB} \eta_{GB} \tag{12}$$

In Eqs. (11) and (12), $P_{ther,t}^{GB}$ is the thermal power output of the gas boiler in the t period. $Q_{gas,t}^{GB}$ is the amount of natural gas burned by the gas boiler in the t period. η_{GB} is the energy conversion efficiency of the gas boiler. λ_{NG} is the heat value of natural gas.

(3) Electric boiler operational constraints

$$P_{ele,min}^{EB} \le P_{ele,t}^{EB} \le P_{ele,max}^{EB} \tag{13}$$

$$P_{ther,t}^{EB} = P_{ele,t}^{EB} \eta_{EB} \tag{14}$$

In Eqs. (13) and (14), $P_{ele,t}^{EB}$ is the electric output of the electric boiler in the t period; $P_{ther,t}^{EB}$ is the thermal output of the electric boiler in the t period; η_{EB} is the energy conversion efficiency of the electric boiler.

(4) EES operating constraints

$$\begin{cases} P_{ch,min}^{EES} u_{ees,t} \le P_{ch,t}^{EES} \le P_{ch,max}^{EES} u_{ees,t} \\ P_{dis,min}^{EES} \left(1 - u_{ees,t}\right) \le P_{dis,t}^{EES} \le P_{dis,max}^{EES} \left(1 - u_{ees,t}\right) \\ S_{min}^{EES} \le S_0^{EES} + \frac{1}{\eta_{ch}^{EES}} \sum_{t'=1}^{t} \left[P_{ch,t'}^{EES} \Delta t\right] - \eta_{dis}^{EES} \sum_{t'=1}^{t} \left[P_{dis,t'}^{EES} \Delta t\right] \le S_{max}^{EES} \\ \sum_{t=1}^{T} \left[P_{ch,t}^{EES} \Delta t\right] - \sum_{t=1}^{T} \left[P_{dis,t}^{EES} \Delta t\right] = 0 \end{cases} \tag{15}$$

In Eq. (15), $P_{ch,t}^{EES}$ is the charging power of EES in the t period. $P_{dis,t}^{EES}$ is the discharging power of EES in the t period. η_{ch}^{EES} is the charging efficiency. η_{dis}^{EES} is the discharging efficiency; S_{max}^{EES} and S_{min}^{EES} are the maximum capacity and minimums capacity of EES; $P_{ch,max}^{EES}$ and $P_{ch,min}^{EES}$ are maximum and minimum of charging power of EES; $P_{dis,max}^{EES}$ and $P_{dis,min}^{EES}$ are maximum and minimum of discharging power of EES.

(5) TES operational constraints

$$\begin{cases} P_{ab,min}^{TES} u_{tes,t} \le P_{ab,t}^{TES} \le P_{ab,max}^{TES} u_{tes,t} \\ P_{rel,min}^{TES} \left(1 - u_{tes,t}\right) \le P_{rel,t}^{TES} \le P_{rel,max}^{TES} \left(1 - u_{tes,t}\right) \\ S_{min}^{TES} \le S_0^{TES} + \frac{1}{\eta_{ab}^{TES}} \sum_{t'=1}^{t} \left[P_{ab,t'}^{TES} \Delta t\right] - \eta_{rel}^{TES} \sum_{t'=1}^{t} \left[P_{rel,t'}^{TES} \Delta t\right] \le S_{max}^{TES} \\ \sum_{t=1}^{T} \left[P_{ab,t}^{TES} \Delta t\right] - \sum_{t=1}^{T} \left[P_{rel,t}^{TES} \Delta t\right] = 0 \end{cases} \tag{16}$$

In Eq. (16), $P_{ab,t}^{TES}$ is the absorbing thermal of TES in the t period; $P_{rel,t}^{TES}$ is the releasing thermal of TES in the t period; η_{ab}^{TES} is the absorbing efficiency; η_{rel}^{TES} is the releasing efficiency; S_{min}^{TES} and S_{max}^{TES} are the minimum capacity and maximum capacity of TES; $P_{ab,max}^{TES}$ and $P_{ab,min}^{TES}$ are maximum and minimum of absorbing power of TES; $P_{rel,max}^{TES}$ and $P_{rel,min}^{TES}$ are maximum and minimum of releasing thermal of TES.

(6) Energy market purchase and sale constraints

$$\begin{cases} 0 \le P_{ele,t}^{BUY} \le u_{ele,t} P_{ele,max}^{BUY} \\ 0 \le P_{ele,t}^{SELL} \le \left(1 - u_{ele,t}\right) P_{ele,max}^{SELL} \\ 0 \le P_{ther,t}^{BUY} \le u_{ther,t} P_{ther,max}^{BUY} \\ 0 \le P_{ther,t}^{SELL} \le \left(1 - u_{ther,t}\right) P_{ther,max}^{SELL} \\ 0 \le Q_{gas,t}^{BUY} \le u_{gas,t} Q_{gas,max}^{BUY} \\ 0 \le Q_{gas,t}^{SELL} \le \left(1 - u_{ther,t}\right) Q_{gas,max}^{SELL} \end{cases} \tag{17}$$

(7) Energy balance constraints

$$\begin{cases} P_{ele,t}^{CHP} + P_{dis,t}^{EES} + P_{ele,t}^{BUY} + P_{ele,t}^{PV} + P_{ele,t}^{WT} \\ = P_{ele,t}^{L} + P_{ele,t}^{EB} + P_{ele,t}^{EL} + P_{ele,t}^{CCS} + P_{ch,t}^{EES} + P_{ele,t}^{SELL} \\ P_{rel,t}^{TES} + P_{ther,t}^{CHP} + P_{ther,t}^{EB} + P_{ther,t}^{GB} + P_{ther,t}^{BUY} = P_{ther,t}^{L} + P_{ab,t}^{TES} + P_{ther,t}^{SELL} \\ sQ_{CH_4,t}^{ME} + Q_{gas,t}^{BUY} = Q_{gas,t}^{L} + Q_{gas,t}^{CHP} + Q_{gas,t}^{GB} + Q_{gas,t}^{SELL} \end{cases} \tag{18}$$

In Eqs. (17) and (18), $P_{ele,t}^{BUY}$, $P_{ther,t}^{BUY}$ and $Q_{gas,t}^{BUY}$ are the electricity, thermal and gas energy purchased from the energy market in the t period of the IES; $P_{ele,t}^{SELL}$, $P_{ther,t}^{SELL}$ and $Q_{gas,t}^{SELL}$ are the electricity, thermal and gas energy sold out of the IES in the t period; $P_{ele,t}^{L}$, $P_{ther,t}^{L}$ and $Q_{gas,t}^{L}$ are the are the electricity, thermal and gas loads of the IES in the t period.

3.3 Adjustable Robust Uncertainty Set

In robust optimization, uncertainty sets are used to describe wind and photovoltaic power generation uncertainty. A finely constructed set yields results closer to reality but increases model complexity and computational burden. Conversely, an overly relaxed uncertainty set leads to overly conservative optimization solutions.

In IES robust dispatch, we choose a cardinality-based uncertainty set mainly because it effectively balances conservativeness and computation efficiency. This set focuses on the number and magnitude of parameter deviations and avoids simultaneous worst-case deviations of all parameters, which significantly reduces conservativeness and offers good flexibility and adaptability.

Robust optimization adopts the uncertainty set to describe the uncertainty. The impact of different uncertainty sets on the optimization results is significant. If the uncertainty set is more refined, the model is more complex and difficult to solve. Conversely, the optimization solution is more conservative when the uncertainty set is broader. The standard uncertainty sets are box uncertainty set and ellipsoidal uncertainty set [34]. Although the box uncertainty set is simple to model and convenient to solve, in the actual scenario, the probability of renewable energy output from this uncertainty set is extremely low. Thus, the optimized solution result using the box uncertainty set is excessively conservative. The ellipsoidal uncertainty set reflects the temporal and spatial correlation of multiple renewable energy outputs, and the modeling is more accurate and consistent with the actual scenario. However, the ellipsoidal uncertainty set increases the complexity of the problem. In order to flexibly adjust the dispatch scheme under different risk preferences, this paper adopts the budget uncertainty set [20] to describe the renewable energy output, as shown in Eq. (19).

$$P_{RE} = \begin{cases} P_{ele,t}^{WT} = \hat{P}_{ele,t}^{WT} + z_{wt,u,t} d_{wt,t} - z_{wt,d,t} d_{wt,t} \\ \sum\limits_{t} z_{wt,t} \le \Gamma_{wt} \\ P_{ele,t}^{PV} = \hat{P}_{ele,t}^{PV} + z_{pv,d,t} d_{pv,t} - z_{pv,d,t} d_{pv,t} \\ \sum\limits_{t} z_{pv,t} \le \Gamma_{pv} \\ \forall t \in T \end{cases} \tag{19}$$

where $P_{ele,t}^{WT}$ and $P_{ele,t}^{PV}$ denote possible values of actual wind and solar outputs within the uncertainty set P_{RE} for time period t; $\hat{P}_{ele,t}^{WT}$ and $\hat{P}_{ele,t}^{PV}$ represent predicted wind and photovoltaic power generation for time period t; $u_{wt,t}$ and $d_{wt,t}$ denote maximum upward and downward deviations of wind output for time period t; $u_{pv,t}$ and $d_{pv,t}$ indicate maximum upward and downward deviations of solar output for time period t; $z_{wt,u,t}$ and $z_{wt,d,t}$ denote 0–1 variables for wind output fluctuations during time period t; $z_{pv,u,t}$ and $z_{pv,d,t}$ denote the 0–1 variables for wind power output fluctuations during time period t. Γ_{wt} and Γ_{pv} are robust adjustable parameters representing the total number of cycles for wind and solar output fluctuations during the scheduling period, ranging from 0 to 24. This value indicates the number of time periods when wind or solar output reaches the boundary of the fluctuation range during the scheduling period, reflecting the system's preference for scheduling risk. A higher value indicates a more conservative scheduling plan, higher system operating costs, and weaker risk tolerance.

The conservatism of the optimization scheme can be adjusted by modifying robust adjustable parameters according to risk preferences. The robustness of the scheduling scheme increases with the rise of the robust adjustable parameters, leading to higher day-ahead operating costs. When Γ_{wt} and Γ_{pv} are set to 0, it indicates deterministic optimization scheduling without considering the uncertainty of wind power and photovoltaic generation. When Γ_{wt} and Γ_{pv} are non-zero, it signifies that the system accounts for the output error between forecasted and actual wind and solar power during scheduling. This error is determined by $u_{wt,t}$, $d_{wt,t}$, $u_{pv,t}$ and $d_{pv,t}$. Therefore, in the IES studied herein, when wind power generation and PV output reach the minimum value within the range, the IES incurs higher operating costs, aligning more closely with the definition of a "worst-case scenario" [29,32].

$u_{wt,t}$, $d_{wt,t}$, $u_{pv,t}$, $d_{pv,t}$, Γ_{wt} and Γ_{pv} are key parameters describing the uncertainty of wind and PV output. $u_{wt,t}$, $d_{wt,t}$, $u_{pv,t}$ and $d_{pv,t}$ are used to explain the fluctuation patterns of wind and PV output. Γ_{wt} and Γ_{pv} determine the duration of output impacts, representing the conservatism and economic efficiency of the scheduling plan. Higher uncertainty values indicate more frequent periods of wind and solar fluctuations, resulting in a more conservative scheduling scheme.

3.4 Two-Stage Robust Optimization Dispatch Model

The two-stage robust optimization dispatch strategy proposed in this paper considers the worst-case scenario of renewable energy output. By leveraging the coupling characteristics of various energy conversion and storage devices within an integrated "wind-solar-hydro-thermal-storage" system, it facilitates energy conversion between electricity, gas, and heat, along with cross-period charging and discharging regulation. This approach mitigates the impact of renewable energy output fluctuations, ensures the supply-demand balance of electricity, gas, and heat loads, enhances the operational stability of the integrated energy system, and reduces overall system operating costs and carbon emissions.

The model employs a two-stage robust optimization approach to address uncertainties in wind and solar power generation, constructing a min-max-min optimization structure to minimize dispatch costs under worst-case scenarios. The first stage of the model is an outer min problem, with optimization variables including the start-up/shut-down status of energy storage devices and the energy purchase/sale status of the system. The second stage is an inner max-min problem, which, after the first stage optimization variables are determined, introduces a set of worst-case renewable energy output scenarios that maximize the system's scheduling cost. Once both the first-stage variables and the second-stage worst-case scenario are fixed, the inner-layer problem transforms into a deterministic optimization aimed at optimizing the output of each unit under the worst-case scenario, ensuring minimal day-ahead scheduling costs. The specific optimization framework is illustrated in Fig. 3.

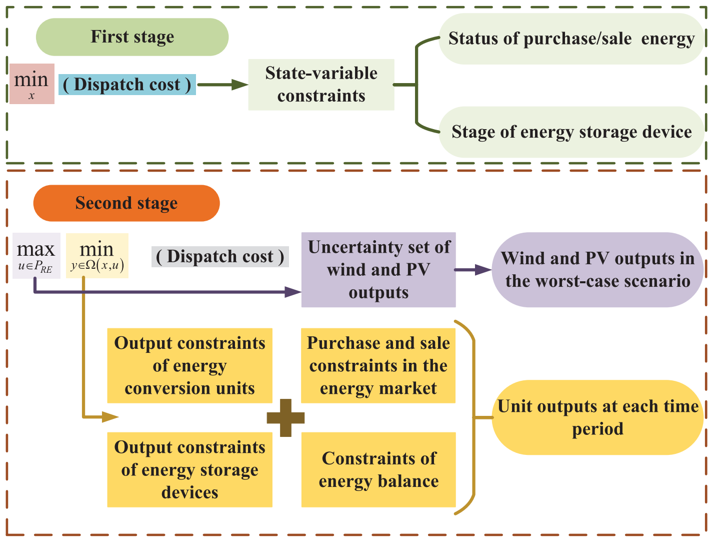

Figure 3: Two-stage robust optimization model

3.4.1 Objective Function

This paper aims to minimize the total operating cost of the IES within an integrated "wind-solar-hydro-thermal-storage" system. The cost components include operating costs of each unit, energy procurement costs from the market, and carbon costs. Based on this objective, a two-stage robust optimization model is formulated to seek the economically optimal dispatch scheme under the worst-case scenario of renewable energy output. The objective function is shown in Eq. (20).

$$min\left\{maxmin\sum_{t\in T}\left[C_O\left(t\right)+C_D\left(t\right)+C_C\left(t\right)\right]\right\} \tag{20}$$

where $C_O\left(t\right)$ is the operating cost of each unit in the system; $C_D\left(t\right)$ is the purchasing cost of electricity, thermal, and natural gas from the energy market; $C_C\left(t\right)$ is the carbon cost in the system, including the cost of CCS operation, carbon capture, carbon storage, and carbon tax.

$$C_O\left(t\right)=\sum_{i}\left(a_i+b_iP_{w,t}^{i}\right) \tag{21}$$

where i denotes each unit in the system; a_i and b_i denote the operation cost factors of each unit. $P_{w,t}^{i}$ is the operating power of each unit in the t period.

$$\begin{aligned}C_D\left(t\right)=&r_{e,t}\left(P_{ele,t}^{BUY}-P_{ele,t}^{SELL}\right)+r_{h,t}\left(P_{ther,t}^{BUY}-P_{ther,t}^{SELL}\right)\\&+r_{g,t}\left(Q_{gas,t}^{BUY}-Q_{gas,t}^{SELL}\right)\end{aligned} \tag{22}$$

where $r_{e,t}$, $r_{h,t}$ and $r_{g,t}$ denote the day-ahead electricity, thermal, and gas prices in the energy market, respectively. $P_{ele,t}^{BUY}$ and $P_{ele,t}^{SELL}$ denote the purchase and sale electricity in the t period. $P_{ther,t}^{BUY}$ and $P_{ther,t}^{SELL}$ denote the purchase and sale thermal in the t period. $Q_{gas,t}^{BUY}$ and $Q_{gas,t}^{SELL}$ are the purchase and sale natural gas in the t period.

$$C_C(t) = k_c P_{ele,t}^{CCS} + k_{sto} Q_{CO_2,t}^{STO} + k_{em}\left(L_{CO_2} P_{ele,t}^{BUY} + Q_{CO_2,t}^{XCCS} - Q_{em}\right) \tag{23}$$

where, k_c and k_{sto} are the carbon capture cost factor, carbon storage cost factor. $P_{ele,t}^{CCS}$ and $Q_{CO_2,t}^{STO}$ are the operating power of CCS and the amount of CO_2 sequestered by CCS in the t period. Besides, $Q_{CO_2,t}^{XCCS}$ and $m_{CO_2} P_{ele,t}^{BUY}$ are the carbon emitted to the atmosphere and the carbon caused by IES purchasing electricity from external market in the t period. k_{em} and L_{CO_2} are carbon emission tax and carbon emission factor for electricity purchase, respectively.

3.4.2 Matrix form of the Dispatching Model

The two-stage robust optimization dispatching model is reformulated based on constraints (1)–(19) and objective function (20). For computational convenience, the model is expressed in compact form. Thus, the matrix form of the proposed two-stage robust optimization dispatching model for IES is shown in Eq. (24).

$$\begin{cases} min\left(\max\limits_{u\in P_{RE}} \min\limits_{y\in\Omega(x,u)} c^T y\right) \\ s.t. \\ Dy \geq d \\ Ey = 0 \\ Fx + Gy \geq h \\ I_u y = u \end{cases} \tag{24}$$

where the first stage is the minimization problem of the outer layer, and the optimization variable is x; the second stage is the max-min problem of the inner layer, and the optimization variables are u and y. The expressions of x, y and u are shown in (25). D, E, F, G and I_u are the coefficient matrices of the variables under the corresponding constraints; d and h are constant column vectors. The two-stage robust optimization dispatching model aims to find the values of uncertain variables u in the worst-case scenario.

$$\begin{cases} x = \left[u_{ees,t}, u_{tes,t}, u_{ele,t} u_{ther,t}, u_{gas,t}\right] \\ y = \left[P_{w,t}^{i}, P_{w,t}^{L}, P_{dis(rel),t}^{m}, P_{ch(ab),t}^{m}, P_{w,t}^{BUY}, P_{w,t}^{SELL}, Q_{gas,t}^{BUY}, Q_{gas,t}^{SELL}\right] \\ u = \left[P_{ele,t}^{PV}, P_{ele,t}^{WT}\right] \end{cases} \tag{25}$$

The proposed model above not only introduces 0–1 integer variables and continuous variables, but also the presence of the min-max-min structure and uncertain parameters increase the difficulty of solve the original problem. Hence, the original model needs to be transformed.

3.5 Model Conversion and Solution

This paper employs the C&CG algorithm [35] to decompose the original problem. The C&CG algorithm continuously introduces variables and constraints related to the subproblem while solving the main problem, thereby obtaining tighter lower bounds on the original objective function to enhance solution speed. Thus, the original problem in Eq. (24) can be decomposed into the main problem (MP) shown in Eq. (26), the outer-layer min problem, and the subproblem (SP) shown in Eq. (27), the inner-layer max-min problem, for alternating solution. The proposed model initially sets the values of the uncertainty variables u to worst-case scenarios. These initial uncertainty values are then substituted into the subproblems. By solving the subproblems, the values of the uncertainty variables under worst-case scenarios are obtained, which are subsequently used to solve MP (26). The min-max SP is transformed into a single-layer maximum problem based on strong duality, aiming to identify the worst-case scenario leading to maximum operational costs, as shown in (27). Notably, the MP serves as a relaxation of the original problem, providing a lower bound; simultaneously, the SP iteratively obtains the worst-case values for uncertainty variables, yielding an upper bound on the optimal solution.

$$MP\begin{cases}\min\limits_{x}\theta \\ s.t. \\ \theta \geq c^T y_k \\ D y_k \geq d \\ Fx + G y_k \geq h \\ I_u y_k = u_k^* \end{cases} \tag{26}$$

$$SP\begin{cases}\max\limits_{u\in P_{RE},\gamma,\lambda,\nu,\pi} d^T\gamma + (h - Fx)^T \nu + u^T\pi \\ s.t. \\ D^T\gamma + K^T\lambda + G^T\nu + I_u^T\pi \leq c \\ \gamma \geq 0, \nu \geq 0, \pi \geq 0 \end{cases} \tag{27}$$

Since the inner min problem within the subproblem is a convex optimization problem, it requires dual transformation to a max problem. However, the resulting max problem contains a bilinear term $u^T\pi$. Therefore, the big M method is employed to linearize it. The final form of the linearized subproblem is shown in (28).

$$\begin{cases}\max\limits_{u\in P_{RE},\gamma,\lambda,\nu,\pi} d^T\gamma + (h - Fx)^T \nu + \hat{u}^T\pi + \Delta u^T B' \\ s.t. \\ D^T\gamma + K^T\lambda + G^T\nu + I_u^T\pi \leq c \\ 0 \leq B' \leq M\cdot B \\ \pi - M\cdot(1 - B) \leq B' \leq \pi \\ \gamma \geq 0, \nu \geq 0, \pi \geq 0 \end{cases} \tag{28}$$

$$\begin{cases}\theta \geq c^T y_{k+1} \\ D y_{k+1} \geq d \\ Fx + G y_{k+1} \geq h \\ I_u y_{k+1} = u_{k+1}^* \end{cases} \tag{29}$$

In this context, Eq. (29) passes the worst-case values of uncertain variables to the main problem to tighten it. θ is the newly introduced auxiliary variable; y_k is the solution to the subproblem after the k-th iteration; u_k^* represents the values of wind and solar power generation obtained under the worst-case scenario after the k-th iteration; $B' = \left[B'_{pv,t}, B'_{wt,t}\right]$ denotes the added auxiliary variable; γ, ν, λ, and π represent the dual form of the constraints for the second-stage minimization problem. A sufficiently large positive real number M is chosen as the upper bound for the dual variable π. Through the above derivation, the two-stage robust optimization model is ultimately decomposed into a mixed-integer linear main problem (26) and a linearized subproblem (28), which can then be solved using the C&CG algorithm, as shown in Fig. 4.

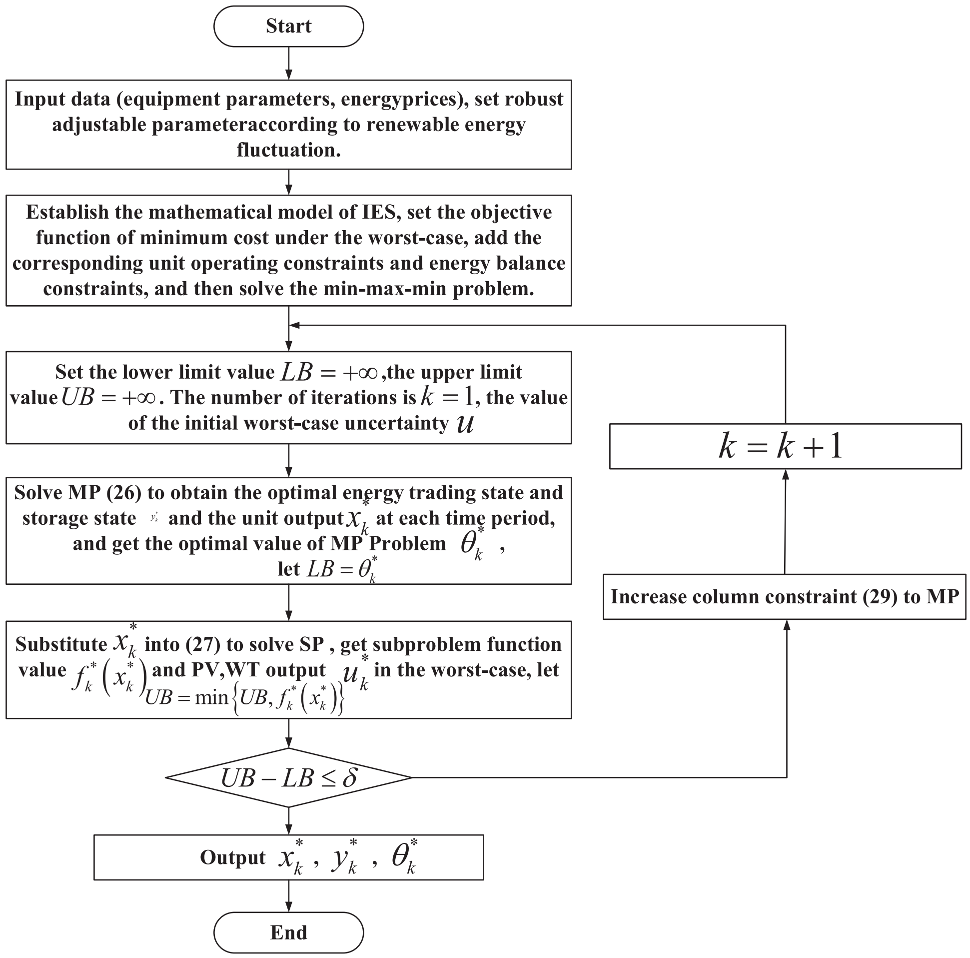

Figure 4: C&CG algorithm running process

As shown in Fig. 4, the implementation process begins by setting a set of initial uncertainty parameters to construct the initial main problem model. After solving the main problem, the current optimal decision scheme is fed into the subproblem. Through a reverse inference mechanism, the subproblem seeks parameter combinations that maximize the deterioration of the system performance metric (operating cost) within the permissible fluctuation range of the uncertainty parameters. This process aims to explore the system's vulnerability boundaries. Its key lies in applying strong duality theory to transform the original two-layer nested optimization problem into a single-layer extremum problem, thereby significantly reducing computational complexity. Once the subproblem identifies the worst-case scenario parameters, the algorithm converts these parameter characteristics into new decision variables and constraint relationships. These are dynamically iterated back into the mathematical model of the main problem, gradually forming a complete enhanced main problem.

4 Case Study

The case analyzes the robustness, economy and environmental benefits of the proposed system based on the results of two-stage robust optimal dispatching of IES containing P2G-CCS equipment. YALMIP invokes the CPLEX solver to solve the proposed two-stage robust optimization problem programmed in MatlabR2018a.

4.1 System Parameters

The day-ahead market price of electricity, thermal, and gas is shown in Table 1. The parameters of units are shown in Tables 2 and 3.

Table 1: Day-ahead energy price in the market

Energy type	Time period	Price
Electrical (¥/MWh)	1:00–6:00	350
	7:00–8:00, 12:00–14:00, 19:00–24:00	500
	9:00–11:00, 15:00–18:00	650
Gas (¥/m³)	1:00–6:00, 20:00–24:00	4.875
	7:00–8:00, 11:00–12:00, 17:00–19:00	8.125
	9:00–10:00, 13:00–16:00	13
Thermal (¥/MWh)	1:00–24:00	400

Table 2: Parameters of energy conversion equipment

Devices	Minimum power (MW)	Maximum power (MW)	Energy conversion efficiency
P2G	0	30	0.85
CCS	0	15	0.8
CHP	10	40	0.9
GB	5	20	0.9
EB	0	10	1

Table 3: Parameters of energy storage equipment

Parameter	Value
Minimum charging and discharging power (MW)	0
Maximum charging and discharging power (MW)	10
Capacity (MWh)	50
Initial Capacity (MWh)	30
Charging and discharging efficiency	0.95

4.2 Data Preparation

The scale of the integrated energy system studied in this paper is park-level, and the case data settings are as follows: Fig. 5 shows 1-year historical output data of a wind farm and a PV plant in a northern China demonstration park, with a sampling interval of one hour. The installed capacities of the wind farm and photovoltaic power station are 80 and 110 MW, respectively. This dataset is used as the original data for simulation. The forecast curves of three types of loads include electric load, thermal load and gas load, are presented in Fig. 6. Based on one year of wind and solar historical data from a comprehensive demonstration park, scenario clustering is used to obtain forecast values of wind and solar power. Considering that the actual PV and wind outputs fluctuate around their forecast values by 15% and 20%, respectively, the forecast and actual output curves of PV and wind are constructed and shown in Fig. 7a,b. The shaded regions represent the uncertainty sets used in this paper. The robust optimization model takes the boundary values of these ranges as the worst-case wind and solar scenarios, while the actual output may lie inside or outside the ranges. Therefore, in the robust optimization process, there is a gap between the wind and solar outputs simulated by the uncertainty set and the actual outputs.

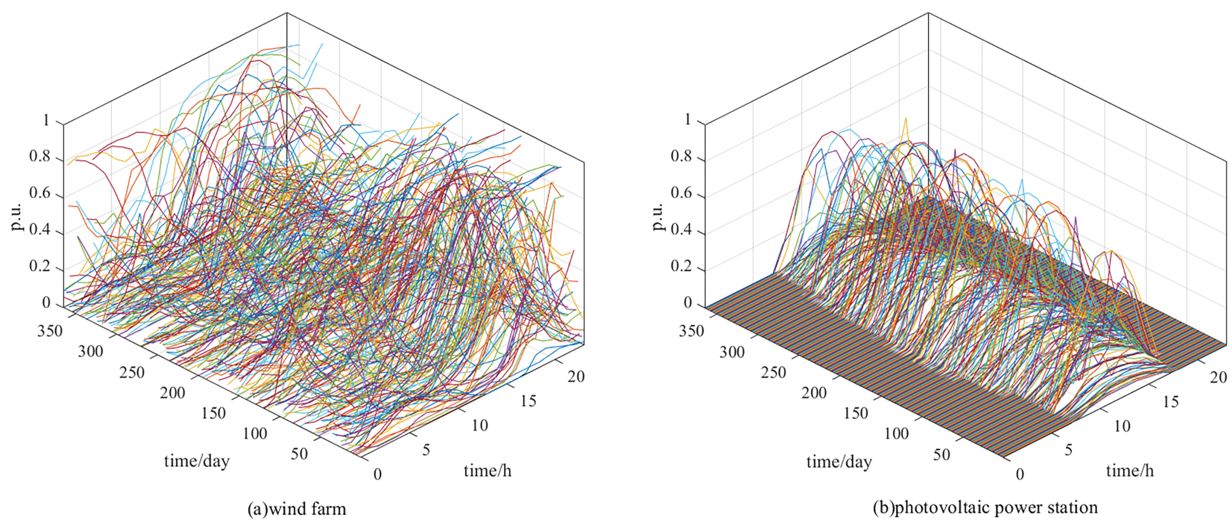

Figure 5: 1-year data of wind farm and photovoltaic power station

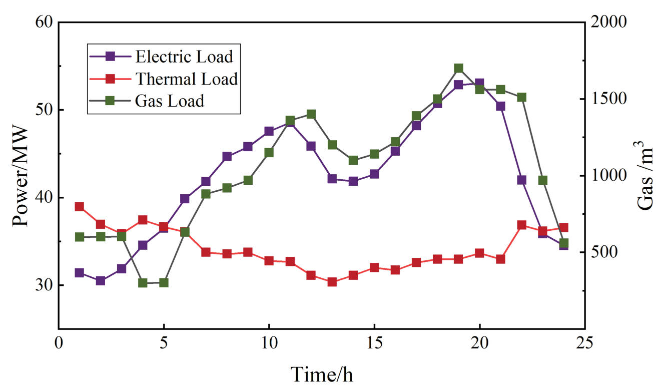

Figure 6: Data of loads

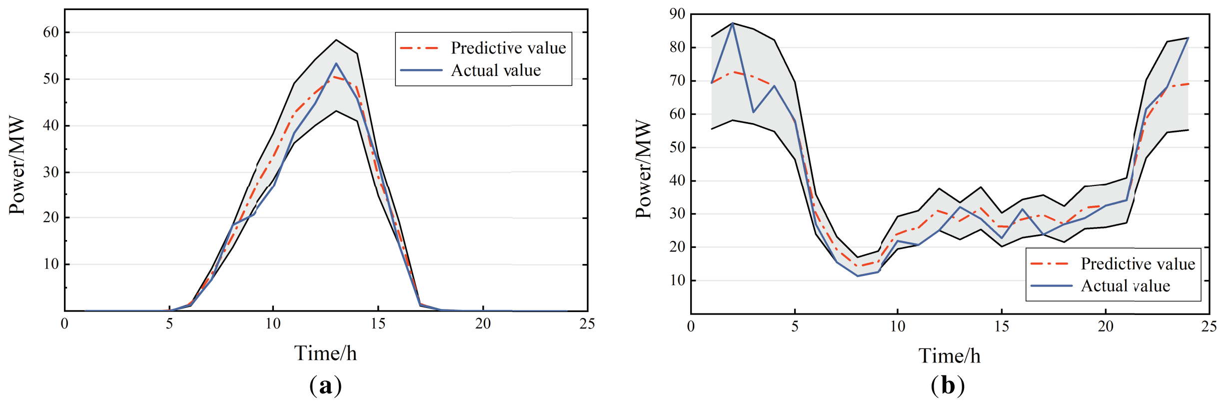

Figure 7: Renewable energy output curve. (**a**) Photovoltaic generator power; (**b**) Wind turbine power

4.3 IES Operation Optimization

4.3.1 Units Operation Analysis

The volatility and intermittency of WT and PV power directly poses strong uncertainty in proposed IES operation. The operation dispatching results of each energy system are shown in Fig. 6 to analyze the integration between each energy system and the operation of each unit under this uncertainty.

Fig. 8a presents the dispatching results for electric system. The proposed IES can consume a large amount of renewable energy, so the electric load is mainly satisfied by the output of the WT and PV. During the hours when renewable energy power is high (1:00–5:00, 11:00–14:00, 22:00–24:00), the excess power is supplied to P2G to produce SNG. At the same time, EES also absorbs excess electricity for charging and storage. Since the electric load demand is low during high wind hours (1:00–5:00, 22:00–24:00) and the thermal load is at peak demand, EB can convert surplus electric energy into thermal energy for satisfying the thermal load. It largely alleviates the wind and photovoltaic curtailment caused by the peak mismatch between the electric demand and thermal demand.

From Fig. 8b, it can be observed that the heat output is mainly supplied by the CHP unit. The proposed IES purchases more thermal energy to satisfy the thermal demand replacing the heat output of the CHP during the hours when renewable energy is sufficient (9:00–16:00). According to the 'heat-setting' feature of CHP, the electric output reduces as the thermal output reduces in order to absorb more renewable energy. The electricity price in the energy market is higher than the thermal price during 9:00–16:00, therefore, utilizing renewable energy can decrease the purchase cost on system electricity energy. It is to be mentioned that GB does not start because the required natural gas must be purchased from the external energy market and the cost of driving GB is much higher than the cost of purchasing heat directly.

As can be seen in Fig. 8c, the surplus electric energy drives the P2G to produce SNG for gas load. The operation of P2G can both reduce the high cost of purchasing gas and utilize the CO_2 captured by the CCS. It is proved that the proposed IES can schedule the P2G-CCS equipment operation flexibly. In addition, the natural gas generated in proposed IES, after satisfying the gas load, the remaining part is supplied to the operation of the CHP.

The proposed IES can realize multi-energy through energy conversion units to efficiently convert electric energy, thermal energy and natural gas. Besides, the IES can also flexibly perform energy storage devices and energy trading mechanisms to absorb more renewable energy, which has a significant renewable energy consumption capability.

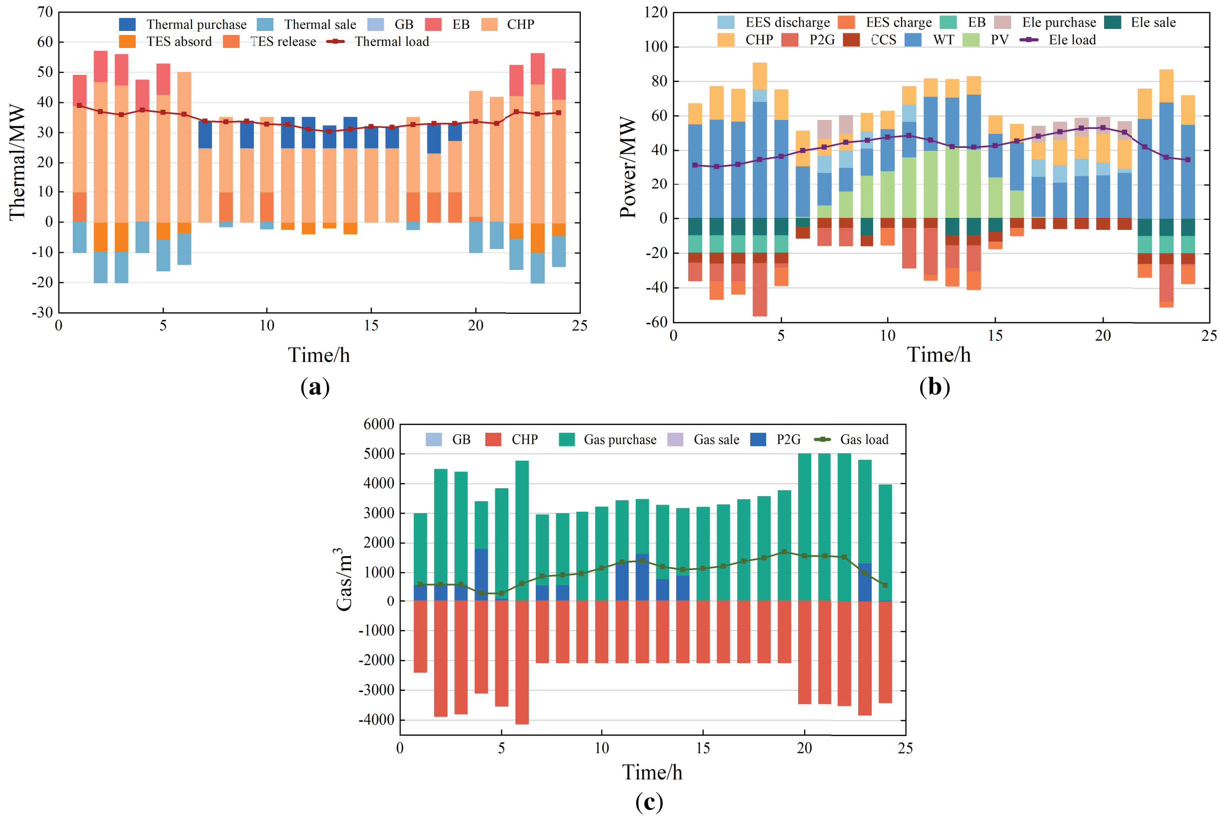

Figure 8: Integrated energy system day-ahead dispatching. (**a**) Electric energy system optimization results of IES; (**b**) Thermal energy system optimization results of IES; (**c**) Natural gas system optimization results of IES

4.3.2 Scenarios Comparison

With the purpose of sufficiently illustrating the impact of the P2G-CCS equipment on the IES optimal operation, and comparing deterministic optimization (DO) and two-stage robust optimization (TRO), the following 4 scenarios are set up.

Scenario 1: Basic scenario. IES traditional economic operation through DO model excluding P2G and CCS.

Scenario 2: Considering the uncertainty of WT and PV output, TRO model is used to optimize the energy system in Scenario 1.

Scenario 3: IES low-carbon economic operation with the introduction of the P2G-CCS equipment through DO.

Scenario 4: Proposed model. Based on scenario 3, both P2G-CCS equipment and TRO are considered.

The results of the IES operating cost under four scenarios are reported in Table 4. Scenario 1 does not have a CCS equipment to capture CO_2, incurring a portion of the carbon tax cost. In addition, due to the weakness of renewable energy consumption capacity in Scenario 1, a large amount of energy curtailment penalty cost is generated. But also because of the overabundance of renewable energy in Scenario 1, a profit of ¥91,080 is obtained through selling electricity to the external market, which is the highest among the four scenarios. With the introduction of P2G-CCS equipment in Scenario 3, the renewable energy consumption capacity and carbon emission reduction are remarkably improved. Compared with Scenario 1, the carbon tax in Scenario 3 is reduced by 57.49%, and the curtailment penalty cost is down to 0, which means that Scenario 3 can achieve fully renewable energy consumption.

Table 4: Day-ahead dispatching cost in different scenarios

Scenario	operating cost (¥)	Energy trading cost (¥)			Carbon related cost (¥)			Curtailment penalty (¥)	Total cost (¥)
		Electricity	Thermal	Gas	Carbon tax	Carbon sequestration	Carbon capture		
1	28,980	−91,080	3680	639,670	25,740	0	0	102,314	709,304
2	28,730	−61,900	11,210	641,170	31,600	0	0	101,350	752,160
3	43,744	−45,230	−20,210	569,480	10,941	10,847	14,186	0	583,760
4	41,374	−18,970	−12,480	599,700	15,926	12,291	14,186	0	652,030

Table 4 reports the dispatch cost results of the IES under four scenarios. In Scenario 1, no CCS equipment is installed, so the system must pay carbon trading costs according to the carbon market rules. Due to relatively weak renewable accommodation capability, Scenario 1 incurs high curtailment penalty costs. At the same time, because large amounts of renewable energy are curtailed, the system obtains the highest profit from selling electricity to the external market ¥91,080 among all four scenarios. In Scenario 3, the introduction of coupled P2G-CCS units significantly enhances renewable energy accommodation and emission reduction. Compared with Scenario 1, the carbon trading cost in Scenario 3 is reduced by 57.49%, and the curtailment penalty cost drops to zero, indicating that renewable energy is fully utilized.

Although operating P2G-CCS requires additional electricity and thus reduces electricity sale profits, the synthetic natural gas produced by P2G supplies the gas network and effectively reduces the cost of natural gas purchases. This greatly decreases the system's dependence on external energy markets. As a result, Scenario 3 achieves the lowest day-ahead total cost among all scenarios. The coordinated operation of P2G-CCS not only improves the environmental performance and supports low-carbon operation of the IES, but also enhances its economic performance, which verifies that the proposed P2G–CCS coupling model is a feasible and promising emerging energy technology.

Scenarios 2 and 4 adopt robust optimization and explicitly consider the intermittency and fluctuation of wind and PV to simulate worst-case renewable outputs. The reduction in renewable generation leads to additional electricity purchases to compensate for the power deficit. Compared with the deterministic Scenarios 1 and 3, the total cost in Scenarios 2 and 4 increases by 5.69% and 11.69%, respectively. In these scenarios, increased electricity purchases raise indirect carbon emissions, and the carbon trading cost rises by 22.76% and 45.56%, respectively. Clearly, when wind and PV uncertainties are considered, the system tends to select more conservative scheduling strategies to ensure operational security. Although the total cost of Scenarios 2 and 4 is higher, this cost represents a deliberate economic compromise by the system to hedge against renewable output uncertainty.

4.4 Model Adjustable Robustness Analysis

4.4.1 Impact of Robustness Adjustment on Economic

This subsection discusses the correlation between the robustness and economy of the proposed model. By varying the robust adjustment parameters, robust optimal dispatching schemes with different degrees of conservatism are developed for comparison. With different levels of conservative dispatch schemes, the impact of robustness on system economy is reflected in the energy purchase cost and the day-ahead dispatch total cost.

From Fig. 9, as the increase of the robust adjustable parameters, it means more periods for PV and WT output to reach the minimum of the fluctuation interval. The day-ahead dispatching cost will gradually get higher under this trend, indicating that the more conservative the optimization scheme tends to be, the worse the economy becomes. The increasing in the cost of energy purchase is the dominant reason for the rise in total cost, electricity purchase cost markedly varies with the increase of robust adjustable parameters, by 64.26% at $\Gamma_{pv} = 13$ $\Gamma_{wt} = 24$ vs. $\Gamma_{pv} = 0$ $\Gamma_{wt} = 0$, and natural gas purchase and thermal purchase cost only by 11.42% and 18.13%. This is attributed to the fact that WT and PV uncertain fluctuations directly affect the electric net and hence the necessity to purchase large amounts of electricity to protect against possible risks.

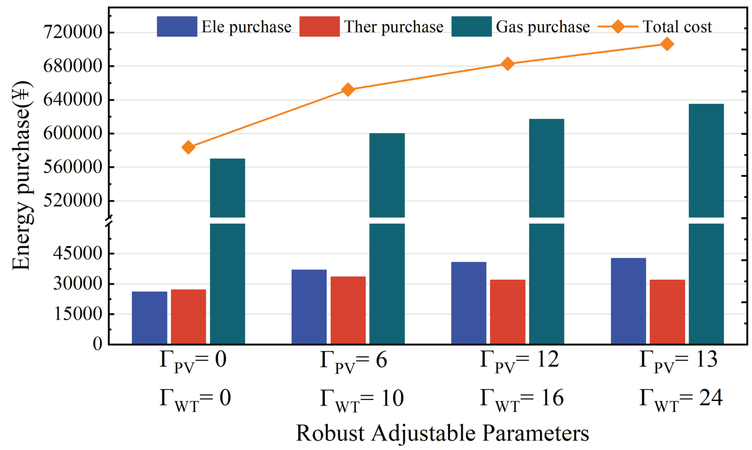

Figure 9: Model cost in different worst-case scenarios

Based on the above analysis, on the one hand, it is proved that the proposed model can effectively adjust the conservativeness of the IES by varying the robust adjustable parameters to obtain optimal strategies under different scenarios. The total cost values can be considered as the reference budget for the corresponding worst-case scenario. On the other hand, energy purchase can improve the system's ability to resist the risk of renewable energy uncertainty, but the 'most conservative solution' is not necessarily the best. It will sacrifice the economy of IES day-ahead dispatch when the optimal solution tends to be conservative.

Therefore, considering the actual fluctuation of WT and PV output, the conclusion is that $\Gamma_{pv} = 6$ $\Gamma_{wt} = 10$ and $\Gamma_{pv} = 12$ $\Gamma_{wt} = 16$ are the most optimal for the dispatching scheme relatively. Since these two schemes not only conform to the actual situations, but also retain the robustness while not overly compromising the system economy. It is suggested that schedulers adopt these two sets of robust adjustment parameters to develop the corresponding scheduling strategies.

4.4.2 Comparison of Optimization Method Economic

After the analysis in the previous section, it is known that the total cost of day-ahead dispatching varies depending on the conservatism of the scheduling strategy. However, as mentioned in Section 4.2, the gap between the simulated and actual power of renewable energy causes a situation in which the energy system needs to purchase and sell electricity for the balance between source-side and load-side. Thus, the intraday balancing cost also impacts the overall energy system economy.

It is assumed that the electricity price of purchase/sale in the intraday market is 1.5/0.5 times that of the corresponding period in the day-ahead market. Table 5 shows the day-ahead, intraday and total costs for the different optimization dispatching methods. It can be observed that the total cost of deterministic optimization is the highest, but the day-ahead scheduling cost is the lowest. The main reason is that deterministic optimization ignores the uncertainty of the renewable energy output, therefore, the energy system needs to expend high cost in the intraday stage to balance the lack of source-side power caused by renewable energy output fluctuations. Compared to deterministic optimization, stochastic optimization is slightly more economical. The proposed two-stage robust optimization has better economic and robustness to cope with the actual output of renewable energy in the intraday stage. For example, the system even profits ¥4300 in the intraday balancing stage and the total cost ¥647,730 is the minimum among three methods. It is worth noting that although the conservative scheme reduces the impact of renewable energy fluctuations in the intra-day stage, it also generates higher day-ahead dispatching cost.

Table 5: Total Cost in different methods

Method		**Day-ahead dispatching cost (¥)**	**Intraday balancing cost (¥)**	**Overall cost (¥)**
Deterministic Optimization		583,760	74,478	658,238
Stochastic Optimization		638,160	19,462	657,622
Two-stage Robust Optimization	Γ_{pv} = **6** Γ_{wt} = **10**	652,030	−4300	647,730
	Γ_{pv} = **12** Γ_{wt} = **16**	684,110	−26,639	657,411

The minimum cost dispatching method is two-stage robust optimization under robust adjustable parameter $\Gamma_{pv} = 6$ $\Gamma_{wt} = 10$. The case results show that it is more reasonable and practical to simulate renewable energy output fluctuations under this set of robust adjustment parameters, as the cost incurred by day-ahead dispatching are not exceedingly high and partial profits are obtained in the intra-day balance.

4.5 Environmental Benefit Analysis

The robustness of system's environmental benefits is worthy of attention and study in the context of low carbon economy operation. This section explores the carbon traces and variation of renewable energy penetration for two-stage robust optimization.

4.5.1 Carbon Traces

In order to investigate the effect of robustness optimization on carbon traces under different worst-case scenarios, four sets of robust adjustment parameters were set and their carbon traces were obtained separately, as shown in Table 6.

Table 6: Carbon traces under different worst-case scenarios

Carbon trace	$\mathbf{\Gamma_{pv} = 0}$ $\mathbf{\Gamma_{wt} = 0}$	$\mathbf{\Gamma_{pv} = 6}$ $\mathbf{\Gamma_{wt} = 10}$	$\mathbf{\Gamma_{pv} = 12}$ $\mathbf{\Gamma_{wt} = 16}$	$\mathbf{\Gamma_{pv} = 13}$ $\mathbf{\Gamma_{wt} = 24}$
From system				
Emission (t)	26.02	26.17	26.31	26.46
Utilization (t)	31.89	22.28	18.52	14.16
Sequestration (t)	72.21	81.82	86.72	91.65

(Continued)

Table 6 (continued)

Carbon trace	$\Gamma_{pv} = 0$ $\Gamma_{wt} = 0$	$\Gamma_{pv} = 6$ $\Gamma_{wt} = 10$	$\Gamma_{pv} = 12$ $\Gamma_{wt} = 16$	$\Gamma_{pv} = 13$ $\Gamma_{wt} = 24$
Total produce (t)	130.12	130.27	131.55	132.26
From market				
Emission (t)	141.19	59.35	65.74	69.57
Carbon tax (¥)	31,254	15,926	17,827	18,968

The carbon emission of the system is slightly affected by the robustness, while the carbon emission generated by electricity purchases from the market is significantly affected. Where, large amounts of electricity need to be purchased intra-day under $\Gamma_{pv} = 0$ $\Gamma_{wt} = 0$, contributing to the highest carbon emission from the energy market at 141.19 t. In contrast, when robust optimization is introduced to the system, the carbon emission from the energy market is reduced by 57.96%. With the increase in robustness, carbon emissions from the energy market also tend to increase, due to more electricity purchases to protect against intraday fluctuations in renewable energy. Besides, the increase in the robust adjustable parameters means that the renewable energy output of the day-ahead dispatching scheme is even insufficient to provide excess power to the P2G. As a result, the carbon produced by the system cannot be utilized for SNG conversion and is instead sequestered.

Considering the impact of carbon emission on the environment and the impact of carbon tax on the overall system economy, the strategy with robust adjustment parameter set $\Gamma_{pv} = 6$ $\Gamma_{wt} = 10$ has relatively well performance in terms of emission reduction. Under this set of robust regulation parameters, the proposed energy system has the lowest carbon emission and carbon tax, which is consistent with the requirements of low-carbon economic operation.

4.5.2 Penetration Analysis

This subsection validates whether the proposed IES with P2G-CCS can consume as much renewable energy as possible and maintain low-carbon economic operation while considering renewable energy fluctuations.

Taking the WT and PV power data from Section 4.2 as the baseline penetration rate scenario (equal to 1.0), Fig. 10 shows the effect of different renewable energy penetration rates on the total cost of IES. The cost of Scenario 2 and Scenario 4 (in Section 4.3.2) are compared under the continuously increasing penetration of renewable energy. When the renewable energy penetration rate is low (from 0.4 to 0.7), the cost of Scenario 4 is higher than that of scenario 2, indicating that the IES containing P2G-CCS does not operate economically with insufficient renewable energy. When the penetration rate is higher than 0.8, the cost of Scenario 4 is lower than that of Scenario 2 and has a continuous decreasing trend. The reason for concern is that when renewable energy resources are abundant enough, Scenario 2 can not consume renewable energy, resulting in a large amount of renewable energy curtailment penalty to raise the total cost. Scenario 4, on the other hand, can still absorb all renewable energy without incurring renewable energy curtailment penalty. As penetration continues to increase, the Scenario 4 cost curve reaches an inflection point where the rate of decline decreases from 5.17% to 3.12%. Owing to the peak in renewable energy absorption capacity of the IES, the system operation incurs a penalty cost for renewable energy curtailment.

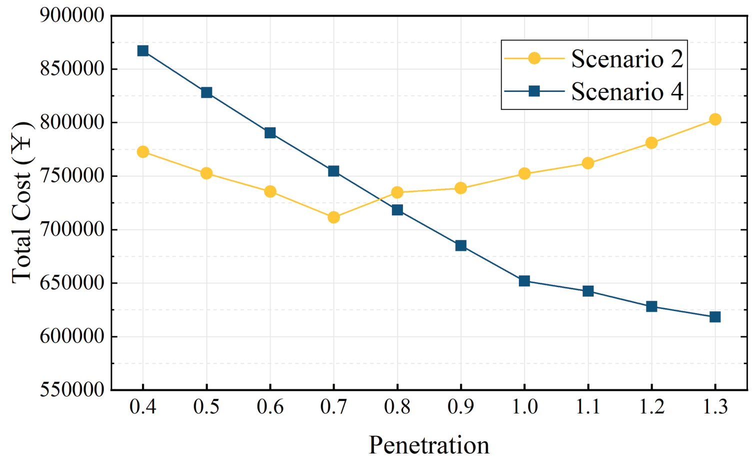

Figure 10: Penetration analysis under different scenarios

Conclusively, IES containing P2G-CCS has excellent renewable energy absorption capacity, and the economic advantages of the proposed energy system are particularly significant at high penetration rates. The increase in renewable energy significantly reduces the units' operating costs, and the economic benefits outweigh the economic damage caused by the abandonment penalty costs of renewable energy. The proposed energy system is robust, economical and environmental efficient at the same time with high renewable energy penetration, which is consistent with the requirements of low carbon economic operation.

5 Conclusion

This paper proposes a two-stage robust optimal dispatch model for a wind-solar-hydro-thermal-storage IES with coupled P2G-CCS. By solving the two-stage robust model using the C&CG algorithm, the following conclusions are drawn based on simulation results and theoretical analysis:

(1) For a park-level IES, constructing a low-carbon economic dispatch model for an electricity–heat–gas system equipped with coupled P2G-CCS devices reduces carbon trading cost by 57.49%, eliminates curtailment penalty cost, and yields a total operating cost of ¥583,760. The results indicate that P2G can flexibly respond to renewable fluctuations by adjusting its input power, effectively enhancing system flexibility. The coupling of P2G-CCS also facilitates renewable energy utilization and enables low-carbon economic operation of the IES.

(2) The proposed two-stage robust optimization with a cardinality-based uncertainty set effectively adjusts the outputs of IES devices to counteract the impact of wind and PV uncertainty while maintaining both robustness and economic and environmental benefits. Compared with deterministic optimization, the two-stage robust optimization reduces total cost by 4.49% and carbon emissions by 57.96%, thereby achieving a balanced optimization among economy, robustness, and low-carbon performance.

(3) As the robustness adjustment parameters increase, the day-ahead dispatch cost of the IES rises continuously. Under extreme uncertainty, the electricity purchase cost in the robust dispatch scheme increases by 64.26% compared with the deterministic scheme with zero uncertainty, because the system must purchase more energy to hedge against renewable risks. Carbon emissions also increase with higher robustness levels. Under extreme uncertainty, the direct emissions are 132.26 t, and emissions associated with day-ahead electricity purchases increase by 42.08%. This is because the robust model reduces P2G utilization as uncertainty grows, ensuring sufficient conventional power to resist renewable fluctuations. Overall, when

the robustness parameters are Γ_{pv} = 6 and Γ_{wt} = 10 set to appropriate moderate values, the dispatch scheme achieves the lowest total carbon emissions and carbon trading cost.

Acknowledgement: The authors gratefully acknowledge the financial support from the Guizhou Science and Technology Department and the National Natural Science Foundation of China. Special thanks are extended to Guizhou Wujiang Hydropower Development Co., Ltd. for the technical support for this research.

Funding Statement: This research was funded by the Research and Application of Key Technologies for Demonstration of Transformation and Promotion for Integrated Development and Operation Methodology of Hydro-Wind-Solar-Storage Integration (Guizhou Science and Technology Cooperation Achievement [2025] General Project 001), Research and Application of Key Technologies for Cascade Clean Energy Development in River Basins (YJPTXM250002) and National Natural Science Foundation of China (52107107).

Author Contributions: Funding acquisition, Jiyuan Liao and Jiangyan Zhao; Investigation, Jiangyan Zhao and Changmao Liu; Methodology, Jiyuan Liao and Xin Li; Software, Jiyuan Liao and Changmao Liu; Validation, Banghong Tang; Writing—original draft, Jiyuan Liao and Jiangyan Zhao; Writing—review & editing, Xin Li; Formal analysis, Zihan Ling. All authors reviewed the results and approved the final version of the manuscript.

Availability of Data and Materials: The authors confirm that the data supporting the findings of this study are available within the article.

Ethics Approval: Not applicable.

Conflicts of Interest: The authors declare no conflicts of interest to report regarding the present study.

References

1. Pawar R, Dalsania KP, Sircar A, Yadav K, Bist N. Renewable energy hybridization: a comprehensive review of integration strategies for efficient and sustainable power generation. Clean Technol Environ Policy. 2024;26(12):4041–58. doi:10.1007/s10098-024-02951-7.
2. Li X, Wang K, Xu M, Fu M, Miao S. Environmental and economic dispatching strategy for power system with the complementary combination of wind-solar-hydro-thermal-storage multiple sources. Front Energy Res. 2024;12:1338657. doi:10.3389/fenrg.2024.1338657.
3. Wang Z, Sun T, Liu N. Risk-managed economic dispatch in hybrid hydrothermal-wind-solar systems: a novel multi-objective optimization approach. Int J Electr Power Energy Syst. 2025;169(4):110753. doi:10.1016/j.ijepes.2025.110753.
4. Li J, Shi L, Fu H. Multi-objective short-term optimal dispatching of cascade hydro-wind–solar-thermal hybrid generation system with pumped storage hydropower. Energies. 2024;17(1):98. doi:10.3390/en17010098.
5. Guo S, Kurban A, He Y, Wu F, Pei H, Song G. Multi-objective sizing of solar-wind-hydro hybrid power system with doubled energy storages under optimal coordinated operational strategy. CSEE J Power Energy Syst. 2021;9(6):2144–55. doi:10.17775/cseejpes.2021.00190.
6. Hu S, Yang Z, Li J, Duan Y. Economic and environmental analysis of coupling waste-to-power technology to integrated energy system (IES) using a two-layer optimization method. J Clean Prod. 2021;325(2):129240. doi:10.1016/j.jclepro.2021.129240.
7. Zhang W, Zhang M, Liu J. Optimal multi-energy storage capacity allocation for electricity-heat-hydrogen-ammonia integrated energy systems with ammonia cycling. Renew Energy. 2026;257(1):124788. doi:10.1016/j.renene.2025.124788.
8. Erixno O, Rahim NA, Ramadhani F, Adzman NN. Energy management of renewable energy-based combined heat and power systems: a review. Sustain Energy Technol Assess. 2022;51(12):101944. doi:10.1016/j.seta.2021.101944.

9. Ma H, Xu F, Chen Q, Hu K, Chen L, Dai Y, et al. Dispatch framework of power system with heat storage facilities in combined heat and power plants for wind power accommodation. IET Renew Power Gener. 2020;14(3):335–43. doi:10.1049/iet-rpg.2019.0595.
10. Xu Y, Liu J, Sun T, Kang H, Hao X. Research on optimal scheduling of integrated energy systems with wind-photovoltaic-biogas-storage considering carbon capture systems and power-to-gas coordination. Energy Eng. 2025;122(8):3155–76. doi:10.32604/ee.2025.065753.
11. Yang C, Dong X, Wang G, Lv D, Gu R, Lei Y. Low-carbon economic dispatch of integrated energy system with CCS-P2G-CHP. Energy Rep. 2024;12:42–51. doi:10.1016/j.egyr.2024.05.055.
12. Mazza A, Bompard E, Chicco G. Applications of power to gas technologies in emerging electrical systems. Renew Sustain Energy Rev. 2018;92(11):794–806. doi:10.1016/j.rser.2018.04.072.
13. Cui D, Ge W, Zhao W, Jiang F, Zhang Y. Economic low-carbon clean dispatching of power system containing P2G considering the comprehensive influence of multi-price factor. J Electr Eng Technol. 2022;17(1):155–66. doi:10.1007/s42835-021-00877-4.
14. Wang Y, Qiu J, Tao Y, Zhang X, Wang G. Low-carbon oriented optimal energy dispatch in coupled natural gas and electricity systems. Appl Energy. 2020;280:115948. doi:10.1016/j.apenergy.2020.115948.
15. Zhang X, Zhang Y. Environment-friendly and economical scheduling optimization for integrated energy system considering power-to-gas technology and carbon capture power plant. J Clean Prod. 2020;276(3):123348. doi:10.1016/j.jclepro.2020.123348.
16. Ma Y, Wang H, Hong F, Yang J, Chen Z, Cui H, et al. Modeling and optimization of combined heat and power with power-to-gas and carbon capture system in integrated energy system. Energy. 2021;236(5):121392. doi:10.1016/j.energy.2021.121392.
17. Zhao C, Guan Y. Unified stochastic and robust unit commitment. IEEE Trans Power Syst. 2013;28(3):3353–61. doi:10.1109/tpwrs.2013.2251916.
18. Zhang D, Jiang S, Liu J, Wang L, Chen Y, Xiao Y, et al. Stochastic optimization operation of the integrated energy system based on a novel scenario generation method. Processes. 2022;10(2):330. doi:10.3390/pr10020330.
19. Di Somma M, Graditi G, Heydarian-Forushani E, Shafie-khah M, Siano P. Stochastic optimal scheduling of distributed energy resources with renewables considering economic and environmental aspects. Renew Energy. 2018;116(12):272–87. doi:10.1016/j.renene.2017.09.074.
20. Nan J, Feng J, Deng X, Guan L, Sun K, Zhou H. A two-stage robust generation expansion planning framework for regional integrated energy systems with carbon growth constraints. Front Energy Res. 2023;11:1106628. doi:10.3389/fenrg.2023.1106628.
21. Gabrel V, Murat C, Thiele A. Recent advances in robust optimization: an overview. Eur J Oper Res. 2014;235(3):471–83. doi:10.1016/j.ejor.2013.09.036.
22. Lorca Á, Sun XA, Litvinov E, Zheng T. Multistage adaptive robust optimization for the unit commitment problem. Oper Res. 2016;64(1):32–51. doi:10.1287/opre.2015.1456.
23. Asghari M, Afshari H, Jaber MY, Searcy C. Enhancing grid stability: a weather-adaptive robust optimization to mitigating renewables curtailment. Renew Sustain Energy Rev. 2025;219(9):115874. doi:10.1016/j.rser.2025.115874.
24. Feng X, Cui L, Ren D, Pan A, Hong J. A new adaptive robust multi-objective optimization algorithm for dispatching of microgrids design. Eng Appl Artif Intell. 2025;159:111715. doi:10.1016/j.engappai.2025.111715.
25. Chen X, Li N. Leveraging two-stage adaptive robust optimization for power flexibility aggregation. IEEE Trans Smart Grid. 2021;12(5):3954–65. doi:10.1109/tsg.2021.3068341.
26. Yang S, Wu H, Song J, Li H, Chen H. Two-stage robust optimization scheduling for integrated energy systems considering ammonia energy and waste heat utilization. Energy Convers Manag. 2024;319(3):118922. doi:10.1016/j.enconman.2024.118922.
27. Yang Z, Wang S, Zhu R, Cui J, Su J, Chen L. Research on regulation method of energy storage system based on multi-stage robust optimization. Energy Eng. 2024;121(3):807–20. doi:10.32604/ee.2023.028167.
28. Li D, Zhang Z, Feng D, Zhou Y, Bai X, Zhao J. Multi-objective two-stage robust optimization of wind/PV/thermal power system based on meta multi-agent reinforcement learning. Int J Electr Power Energy Syst. 2024;162(1):110273. doi:10.1016/j.ijepes.2024.110273.

29. Liu Y, Guo L, Wang C. Economic dispatch of microgrid based on two stage robust optimization. Proc CSEE. 2018;38(14):4013–22.
30. Li C, Qin W, Wang J, Zhu X, Lu S, Li J. A two-stage robust optimization for multi-timescale coordinated control of electro-hydrogen energy storage and demand response. J Energy Storage. 2026;141(12):119077. doi:10.1016/j.est.2025.119077.
31. Li Y, Zhang F, Li Y, Wang Y. An improved two-stage robust optimization model for CCHP-P2G microgrid system considering multi-energy operation under wind power outputs uncertainties. Energy. 2021;223(9):120048. doi:10.1016/j.energy.2021.120048.
32. Wang G, Wu Y, Qian X, Zhao Y. Distributed robust scheduling optimization of wind-thermal-storage system based on hybrid carbon trading and Wasserstein fuzzy set. Energy Eng. 2024;121(11):3417–35. doi:10.32604/ee.2024.052268.
33. Li X, Li T, Liu L, Wang Z, Li X, Huang J, et al. Operation optimization for integrated energy system based on hybrid CSP-CHP considering power-to-gas technology and carbon capture system. J Clean Prod. 2023;391(9):136119. doi:10.1016/j.jclepro.2023.136119.
34. Bertsimas D, Sim M. The price of robustness. Oper Res. 2004;52(1):35–53. doi:10.1287/opre.1030.0065.
35. Zeng B, Zhao L. Solving two-stage robust optimization problems using a column-and-constraint generation method. Oper Res Lett. 2013;41(5):457–61. doi:10.1016/j.orl.2013.05.003.